Title: Influence of the climatic conditions on the hygrothermal performance of autoclaved aerated concrete masonry walls

Authors: André D. Trindade, Guilherme B.A. Coelho and Fernando M.A. Henriques

Journal: Journal of Building Engineering

DOI: https://doi.org/10.1016/j.jobe.2020.101578

Please cite this article as: A. D. Trindade, G.B.A. Coelho, F.M.A. Henriques, Influence of the climatic conditions on the hygrothermal performance of autoclaved aerated concrete masonry walls, Journal of Building Engineering (2021) https://doi.org/10.1016/j.jobe.2020.101578

This is an unedited manuscript of: *Influence of the climatic conditions on the hygrothermal performance of autoclaved aerated concrete masonry walls* which has been accepted for publication in *Journal of Building Engineering*.

Influence of the climatic conditions on the hygrothermal performance of autoclaved aerated concrete masonry walls

André D. Trindade, Guilherme B.A. Coelho*, Fernando M.A. Henriques

Departamento de Engenharia Civil, Faculdade de Ciências e Tecnologia, Universidade NOVA de Lisboa, Quinta da Torre, 2829-516 Caparica, Portugal, Tel.: +351 212948580; fax: +351 212948398

* Corresponding author. E-mail addresses: g.coelho@campus.fct.unl.pt (G. Coelho)

Abstract

The energy performance of buildings has undergone major developments over the last few years. Due to increasingly demanding regulations, new technologies and constructive solutions have been sought to make buildings more energy efficient. Autoclaved aerated concrete (AAC) is a sustainable building material that provides a suitable solution to this problem. However, the hygrothermal behavior of AAC masonry walls is the subject of little discussion throughout the scientific community. The paper focuses on identifying the influence of climatic conditions, as well as the effect of surface layers or insulation systems on the hygrothermal performance of exterior walls made of AAC. For the purpose of this study, several constructive solutions were analyzed in different climatic settings, namely Munich, Germany; Stockholm, Sweden; and San Francisco, U. S. A. The effects of applying different types of render/plaster layers or external thermal insulation system on AAC walls was also determined using hygrothermal software. In addition, the damage potential of frost and rainwater were assessed to better comprehend how these walls behave. The results showed that the overall performance of AAC wall systems and frost damage potential was found to be greatly influenced by the hygric properties of the exterior render. Additionally, it was shown that calculating the thermal transmittance in steady-state conditions can lead to gross underestimations compared to transient models. The results indicate that the EPS and XPS insulated walls were susceptible to moisture increase, due to rainwater leakage, unlike the MW insulated wall, which dried significantly faster.

Keywords: Computational simulation, Autoclaved aerated concrete, Thermal transmittance, Hygrothermal performance, Frost damage.

1. Introduction

Autoclaved aerated concrete (AAC) is a lightweight building material commonly used in Europe, known for its thermal insulation and acoustic absorption properties. This concrete is composed of Portland cement, lime, sand or fly ash, and aluminum powder. One key characteristic of AAC is its hygric properties, which are highly dependent on water content due to its highly porous media [1]. As a result, high water content values can significantly decrease the thermal performance of AAC, which may justify why its application has been met with such a varying rate of success throughout the world [2,3].

The hygrothermal performance of AAC masonry walls has been previously investigated. For instance, Kočí *et al.* [4] performed a computational analysis focused on potential frost damage, aimed at increasing the service life of exterior thermal insulation systems suitable for AAC building envelopes in cold regions. Jerman *et al.* [3] studied the hygric and thermal properties of three commercially produced AAC products with different bulk densities and compressive strengths, as well as their basic characteristics and durability. The results showed that the thermal conductivity of AAC could be as much as six times higher in a state of capillary water saturation compared to dry conditions.

Additionally, Drochytka *et al.* [5] studied the hygrothermal performance of AAC blocks made from fly ash, as opposed to sand-based material. The fly ash-based AAC demonstrated slightly larger moisture sorption; however, its thermal conductivity was found to be less moisture dependent. Further, Qiu *et al.* [6] analyzed moisture transport across bonded and natural contact interfaces between AAC and mortar. The results showed that, for both interfaces, the assumption of a perfect hydraulic contact may result in significant errors when predicting moisture transport. More recently, Künzel [7] investigated driving rain protection of AAC walls by focusing his research on the hygric parameters of the exterior render. The results showed that the exterior surface layer should include specific limits for water absorption and diffusion resistance, and that these properties should not degrade with time.

Fully understanding the hygrothermal performance of AAC is crucial for designers and manufacturers, in order to avoid misinterpretation of the design data. The aim of this paper is to analyze the influence of climatic conditions on the hygrothermal performance of AAC wall envelopes. The performed analyses were based on the variation of hygrothermal parameters, namely water content, heat flux, moisture flux, thermal conductivity, and potential frost damage.

This paper analyses the influence each layer has on the hygrothermal performance of the AAC block. Masonry walls consist of a series of layers that comprise the entire wall assembly. In order to meet strict building regulations, understanding how each individual material affects the hygrothermal performance of the overall wall is necessary. Hence, simulations were first carried out for an AAC masonry wall without any coatings. Afterwards, the hygrothermal changes associated with the application of plaster and render layers were identified, followed by the application of an ETICS.

To assess different climatic conditions, three locations with distinct characteristics were chosen for this study: San Francisco, U. S. A. has mild winters, fairly cool summers, and moderate precipitation. Stockholm, Sweden has warm summers, cold winters, and moderate precipitation. Lastly, Munich, Germany has low annual average temperatures and high precipitation all year round. The interior climate was defined through sine curve parameters for residential buildings with medium moisture loads, which adequately represents the majority of the residential building stock for these regions.

The selected walls assemblies were tested in WUFI® [8], which is a hygrothermal simulation software widely accepted by the scientific community, as it has been validated by numerous independent studies and used in several studies, as well. For example, Villman et al. [9] showed that the moisture transport models, which include both vapor and liquid transport for drying in cement mortars, yielded results with sufficient accuracy for practical applications. Alev et al. [10] validated the simulation model for test walls based on measured results. Temperature, relative humidity, and heat flux showed good agreement between measured and calculated results. Nascimento et al. [11] analyzed the wind driven rain (WDR) incidence parameters obtained by hygrothermal simulation, presenting a methodology for obtaining the most critical orientation in hygrothermal design. Coelho and Henriques [12] analyzed the influence of WDR on the hygrothermal performance of solid brick walls and corroborated the notion that WDR is one of the main sources of moisture in high capillary water uptake walls. Ramos et al. [13] investigated the risk of interstitial condensation and provided a methodology to account for this phenomenon in hygrothermal design. Additionally, this software complies with the benchmark test defined by the European Standard EN 15026 [14]. The governing equations that WUFI uses to determine the heat and moisture transfer are coupled through two variables, temperature and relative humidity, from which all other variables can be derived [15].

Damage functions are commonly used in hygrothermal simulations in order to assess the severity of environmental loads in a given region, thus, allowing a comparison between the effectiveness of different constructive solutions. Although frost damage is a difficult physical mechanism to quantify [16], several damage functions have been developed which allow a relative assessment of this phenomenon, namely the number of critical freeze-thaw cycles, *Time-of-Frost,* and the *Amount-of-Frozen-Water* [17]. In this paper, the authors focused the analysis on a point in the AAC layer, 2 mm under its exterior surface, which is considered a characteristic position for frost damage to occur [18]. Additionally, frost damage is considered likely to occur when moisture content is over the hygroscopic range, which is adequate for hygrothermal simulations [19].

Thermal conductivity is a fundamental parameter to characterize the hygrothermal performance of a constructive solution, given that a higher thermal transmittance corresponds to a higher heat flux density and, thus, greater heat losses. In porous building materials, thermal conductivity is highly dependent on water content and changes according to ambient conditions [12]. In general, a steady-state analysis is useful when the temperature of the material does not change with time. However, for the purpose of building physics, this simplified model may lead to unrealistic results due to the varying effects of prevailing winds and solar radiation. In the present paper, this variance was also investigated.

The research developed in this paper was undertaken to determine the effect, for each layer, of the wall assembly on the hygrothermal performance of the wall system, as well as the importance of climatic conditions. Consequently, an analysis was developed for various wall systems, comprised of different rendering materials, as well as the application of an external thermal insulation system. The importance of climatic conditions was determined by simulating the models on three different climate settings with very distinct characteristics, namely Munich, Germany; Stockholm, Sweden; and San Francisco, U. S. A.

2. Methodology

The methodology presented here describes the procedures used to analyze the influence of climatic conditions on the hygrothermal performance of AAC wall envelopes and to identify the importance of each layer of the wall assembly.

A masonry wall system must allow for proper control of moisture, vapor, and heat transmission, and the hygrothermal performance of each layer of the wall assembly plays a significant role. This analysis is structured into four main phases.

i. First, an analysis was developed for an unrendered AAC masonry wall, in order to determine the importance of wall thickness and orientation as a function of climatic conditions. This was achieved by simulating different wall assemblies, varying only the AAC layer thickness and façade orientation. To represent the typical constructive solutions employed in the studied regions, the AAC block thicknesses considered were 200, 240, 300, and 365 mm, as seen in Figure 1. Frost damage potential was also analyzed in Munich and Stockholm. In this phase, the 200 mm AAC wall with the most critical orientation in each climate was chosen for further assessment [20], designated as the *standard case*.

ii. The hygrothermal changes imposed by the application of a plaster and render layer were investigated. Lime, lime-cement, and cement renders were considered on the exterior surface, while gypsum plaster was considered on the interior surface. The hygrothermal changes caused by the application of the aforementioned layers were analyzed relative to the unrendered AAC wall (i.e. standard case). Additionally, different render thicknesses were considered, in order to identify the hygrothermal changes associated with the increase of thickness, specifically 5, 15, and 30 mm.

iii. The hygrothermal changes imposed by the application of an ETICS were investigated. The simulations were carried out for three insulation materials commonly used in this type of systems: mineral wool (MW), expanded polystyrene (EPS), and extruded polystyrene (XPS). Insulation layer thicknesses of 20, 100, and 200 mm were investigated with a 1.5 mm resin finish coat on the exterior surface, which is representative of the current construction practice in the studied regions [21–23].

iv. Lastly, the importance of rainwater leakage on the water content of AAC masonry walls was investigated. Different rainwater leakage values were investigated: 0 % of the wind-driven rain, assuming a perfectly watertight system, without any cracks or gaps; 1 %, the default value according to ANSI/ASHRAE Standard 160 [24]; 3 %; and 5 %, assuming a worst-case scenario [25].

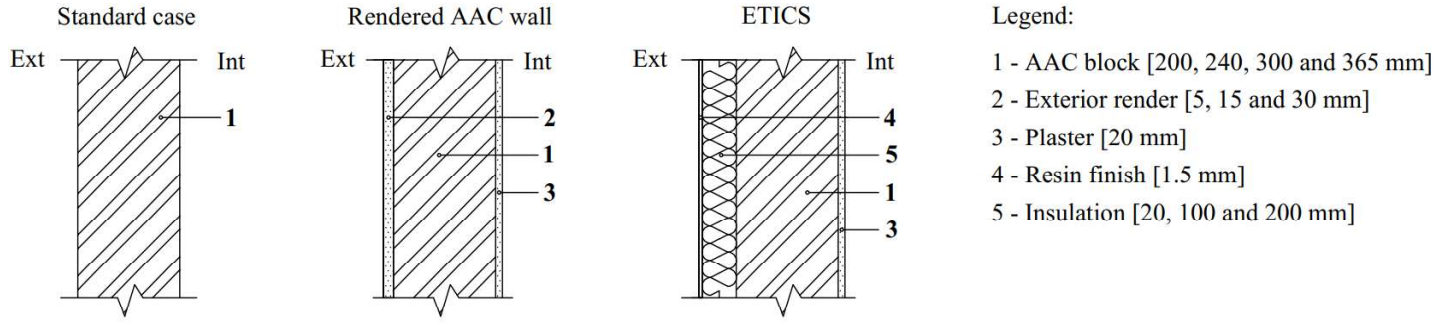

Figure 1. Simulated wall assemblies.

The results obtained from WUFI® [8] were compared against the results from Delphin [26] for the same climate and wall assembly. The obtained results presented a similar trend in terms of water content annual variance, validating the WUFI results.

2.1 Thermal and hygric parameters

Thermal conductivity is a fundamental parameter used to characterize the hygrothermal behavior of porous building materials. However, its measurement is complex due to a large dependency on several factors. WUFI calculates the moisture-dependent thermal conductivity of mineral building materials through the following equation [15]:

$$\lambda(w) = \lambda_0 \left(1 + b \cdot \frac{w}{\rho_s}\right) \quad (1)$$

where λ is the thermal conductivity of the moist building material in W/(m K), λ_0 is the thermal conductivity of dry building material in W/(m K), b is the thermal conductivity supplement in %/(M.-%) (as defined by *Künzel* in Ref. [15]), w is the water content in kg/m^3, and ρ_s is the bulk density of the dry building material in kg/m^3. Thermal transmittance of the wall (i.e. U-value) was calculated from moisture-dependent thermal conductivity, and all the simulations were run for a period of 5 years, in order to achieve a state of dynamic equilibrium. As such, the U-values presented in this research refer to the last year of the simulation period.

Water vapor transport through porous building materials is obtained through Fick's law of diffusion, where vapor pressure is the main driving gradient. Given that there is greater resistance to vapor diffusion in porous media compared to an air layer, a water vapor diffusion resistance factor has to be taken into account, characteristic of each building material [15]. As a result, the diffusion flux density is obtained through the following equation:

$$g_v = -\frac{\delta_{p,a}}{\mu} \cdot \frac{\partial p_v}{\partial x} \quad (2)$$

where g_v is the water diffusion flux density in kg/(m^2 s), $\delta_{p,a}$ is the water vapor permeability in the air in kg/(m s Pa), μ is the water vapor diffusion resistance factor (adim.), and p_v is the water vapor partial pressure in Pa.

The liquid transport coefficient for a given construction material can be obtained experimentally and is governed by the following equation:

$$A = \frac{M_1 - M_0}{S \cdot \sqrt{t}} \quad (3)$$

where A is the liquid transport coefficient in kg/(m^2 s$^{1/2}$), $M_1 - M_0$ describes the difference in mass in kg, S is the surface area in m^2, and t is time in seconds. It should be noted that moisture transport in the interface between two capillary-active materials is considered perfect in WUFI [8]. In reality, however, there may be transfer resistance, which reduces moisture transport [27].

2.2 Damage functions

When the temperature drops below the freezing point, ice formation occurs with an inherent volume increase that may cause damage to the porous structure of the material if its pores are near saturation. Under these circumstances, there is no capillary suction, and the vapor transport is hindered when at least 60% of the pores are filled [15]. The effects of freeze-thaw cycles can cause damage to the exposed surface, depending on the pore structure and tensile strength of the material. According to *Straube* [20], the two factors that influence frost damage most are the water content on freezing and the number of freeze-thaw cycles.

In this paper, the authors focused the analysis on a point in the AAC layer, 2 mm under its exterior surface, which is considered a characteristic position for frost damage to occur [18]. Additionally, frost damage is considered likely when moisture content is over the hygroscopic range, which is adequate for hygrothermal simulations [19].

The number of critical freeze-thaw cycles represents the number of cycles that occur while the water content is over the hygroscopic range. In this paper, it was assumed that, for a valid freeze-thaw cycle to occur, the freezing must take at least 2 hours, while two consecutive freeze-thaw cycles must be separated by a thawing period of at least 2 hours [17]. Critical freezing occurs when temperature drops below 0 ºC and the moisture content is over the hygroscopic range for AAC (i.e. 36.8 kg/m^3).

Time-of-Frost (TOF) is a damage function developed by Kočí *et al.* [17] that calculates the number of hours a year the conditions for ice formation are favorable. This damage function assesses the severity of a climate with respect to frost damage. TOF can be expressed in hours or by a percentage of the year:

$$TOF = \sum_{i=1}^{8760} (T_i < T_L \wedge w_i > w_L) \tag{4}$$

where T_i is the hourly value of temperature in ºC, T_L is the critical temperature in ºC, w_i is the hourly value of water content in kg/m^3, and w_L is the critical water content in kg/m^3. The critical temperature (T_L) depends on the pore size distribution of the analyzed material and the possible concentration of soluble salts [8]. However, in WUFI, it is not possible to take these factors into account. Hence, as a simplification, a critical temperature of 0 ºC was assumed, which allows for a safer assessment of the results given that, in reality, ice formations occurs for slightly lower temperatures.

The Amount-of-Frozen-Water (AFW) [17] calculates the amount of liquid water retained in the investigated point under the critical temperature during the year. This function assumes that when the temperature drops below the freezing point, any liquid water present in the material accounts for ice formation. Although, this is not physically true because there is still some liquid water in the smaller pores. This function allows for a relative assessment:

$$AFW = \sum_{i=1}^{8760} w_i (T_i < T_L \wedge w_i > w_L) \tag{5}$$

where T_i is the hourly value of temperature in ºC, T_L is the critical temperature in ºC, w_i is the hourly value of water content in kg/m^3, and w_L is the critical water content in kg/m^3.

2.3 Simulation settings

In order to perform the selected simulations, the building materials presented in Table 1 were used to constitute the selected wall assemblies. These materials were characterized by Fraunhofer IBP and MASAE. Lime mortar and cement mortar were selected for this study because they allowed us to analyze a wide range of mortars, since their hygric characteristics are very far from each other (for instance, the water absorption coefficient of lime mortar is 47 times higher than the water absorption coefficient of cement mortar).

In order to account for rainwater leakage in the ETICS simulations, a moisture source was introduced into the substrate layer, between the insulation material and AAC block [23]. The moisture source was set to 1 % of the wind-driven rain incident on the exterior surface, in accordance with ANSI/ASHRAE Standard 160 [24].

The exterior heat resistance was considered wind dependent. The short-wave radiation absorptivity varies according to the material of the exterior surface (0.65 for AAC and 0.40 for all other materials considered of normal brightness). A ground short-wave reflectivity standard value of 0.2 was adopted. The adhering fraction of rain was set to 0.7, which is adequate for most vertical walls [8]. The heat resistance of the interior surface was set to the standard value of 0.125 m^2 K/W. All simulations were run until a state of dynamic equilibrium was reached; thus, a time period of 5 years was sufficient.

Table 1. Properties of the materials analyzed in the present paper (data taken from WUFI's database [8]).

Material	Bulk density	Porosity	Water absorption coefficient	Thermal conductivity, Dry	Water vapor diffusion resistance factor
	[kg/m^3]	[m^3/m^3]	[kg/m^2 s$^{0.5}$]	[W/m K]	[-]
AAC block	400	0.81	0.056	0.100	7.9
Lime	1600	0.30	0.047	0.700	7.0
Lime-cement	1900	0.24	0.017	0.800	19.0
Cement	1436	0.42	0.001	0.608	25.0
Resin finish	1100	0.12	0.001	0.700	1000.0
Gypsum plaster	850	0.65	0.287	0.200	8.3
MW	60	0.95	—	0.040	1.3
EPS	15	0.95	—	0.040	30.0
XPS	40	0.95	—	0.030	100.0

The boundary conditions for the exterior surface are defined from the climate files available in the WUFI database for

Munich, Germany; Stockholm, Sweden; and San Francisco, U. S. A.

The Köppen climate classification is one of the most widely used climate classification systems [28]. It was first published by Wladimir Köppen in 1884 and has been updated throughout the years by many other authors. The Köppen-Geiger classification divides climates into five main climate groups, represented by the first letter: A (equatorial), B (arid), C (warm temperate), D (snow), and E (polar). The second letter represents the precipitation: W (desert), S (steppe), f (fully humid), s (summer dry), w (winter dry), and m (monsoonal). Lastly, the third letter represents the temperature: h (hot arid), k (cold arid), a (hot summer), b (warm summer), c (cool summer), d (extremely continental), F (polar frost), and T (polar tundra). For example, a climate classified as Cfa is considered to be a warm temperate climate, fully humid with hot summers.

Munich is classified as Cfb (warm temperate, fully humid with warm summers), characterized by cold winters with no dry season, warm summers, and heavy precipitation all year round. Stockholm has warm summers, severe winters, no dry season, and a strong seasonality with a Köppen-Geiger classification of Dfb (snow, fully humid with warm summer). Lastly, San Francisco has mild winters, dry summers, and moderate seasonality. It is classified as Csb (warm temperate, summer dry with cool summer). The wind-driven rain and solar radiation distribution for each of these three climates is provided in Figure 2 and Figure 3.

In the scope of this paper, it was necessary that the interior climate conditions remained the same for all the simulations, so the only variables were the exterior climate settings [12]. For this reason, the interior boundary conditions were defined using sine curve parameters for residential buildings with medium moisture loads. These values are available in Table 2.

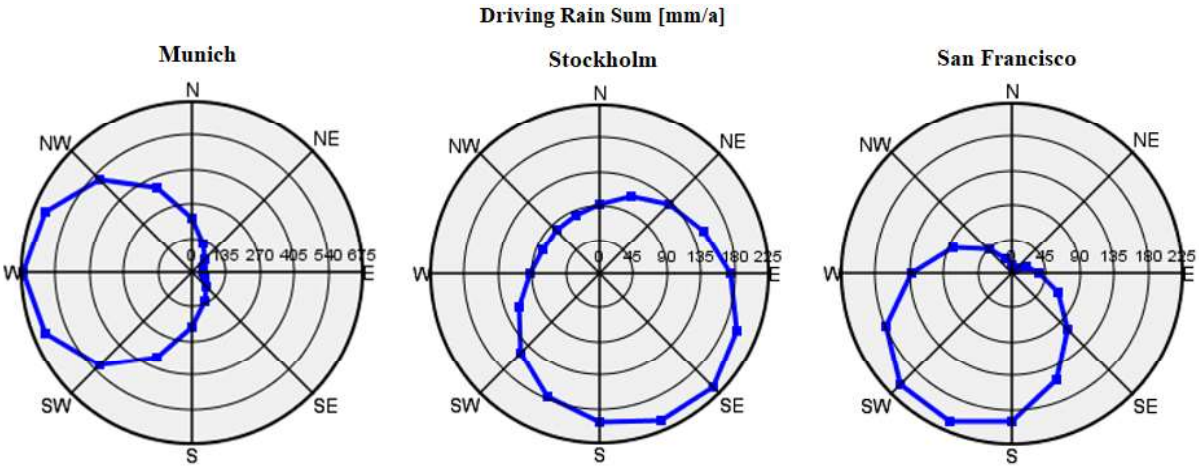

Figure 2. Wind-driven rain directional distribution (mm/a) in Munich, Stockholm, and San Francisco (data taken from WUFI's climate analysis [8]).

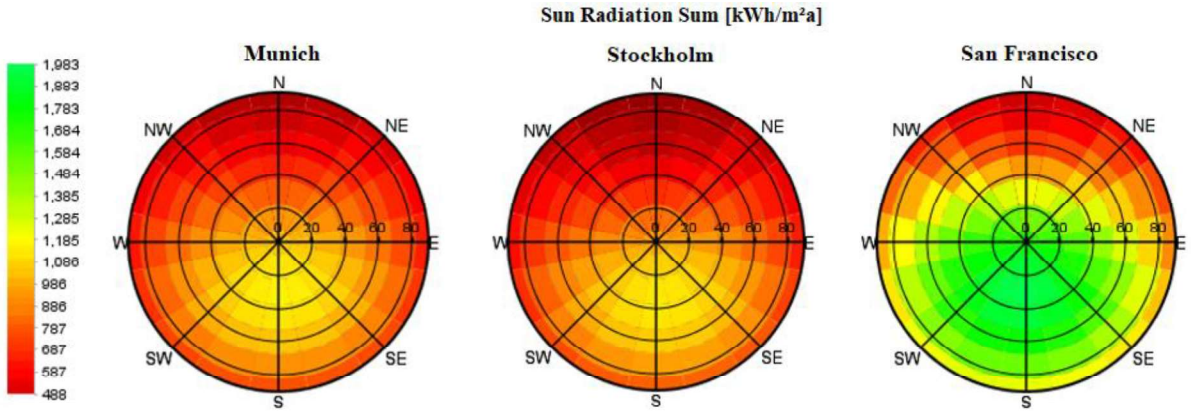

Figure 3. Solar radiation directional distribution (kWh/m^{2}a) in Munich, Stockholm, and San Francisco (data taken from WUFI's climate analysis [8]).

Table 2. Temperature and relative humidity for the simulated climates.

Outdoor climate		Munich	Stockholm	San Francisco	Indoor climate
Temperature [ºC]	Min.	-17.9	-18.6	1.1	20.0
	Max.	30.6	29.4	37.2	22.0
	Mean	8.0	6.8	12.6	21.0
Relative humidity [%]	Min.	21.0	22.0	15.0	40.0
	Max.	100.0	99.0	100.0	60.0
	Mean	78.2	78.6	73.7	50.0

3. Results and discussion

3.1 Uncoated AAC wall

3.1.1 Orientation

The water content of AAC masonry walls should be carefully monitored, as it impairs thermal performance and accelerates ageing and degradation [23]. When exposed to the natural climate without any rain protection measures, the moisture equilibrium is governed by alternating events of rain and sunshine [29]. Figure 4 shows the annual average water content in each climate as a function of façade orientation. It can be seen, for each climate, that the façade with the highest wind-driven rain load also reaches the highest annual average water content: west in Munich, southeast in Stockholm, and southwest in San Francisco. This further corroborates the notion that wind-driven rain is one of the main sources of moisture in high capillary uptake walls, such as AAC masonry walls.

However, solar radiation also plays a significant role, since it affects the drying potential of the façade. Figure 5 shows the variation of water content for the northwestern- and southwestern-oriented facades in Munich. Even though both cases are subjected to a similar amount of wind-driven rain (ca. 180 l/m^{2}y), the variation of water content is quite different. The

southwestern-oriented façade reaches the lowest values overall. This behavior is due to the higher amount of solar radiation on the southern direction (see Figure 3), which leads to a higher average surface temperature and, thus, a faster drying process. Therefore, for similar wind-driven rain loads, solar radiation becomes a predominant factor on the hygric behavior of the masonry wall. Henceforward, the façade with the highest wind-driven rain load in each climate was chosen for further assessment and designated as the standard case.

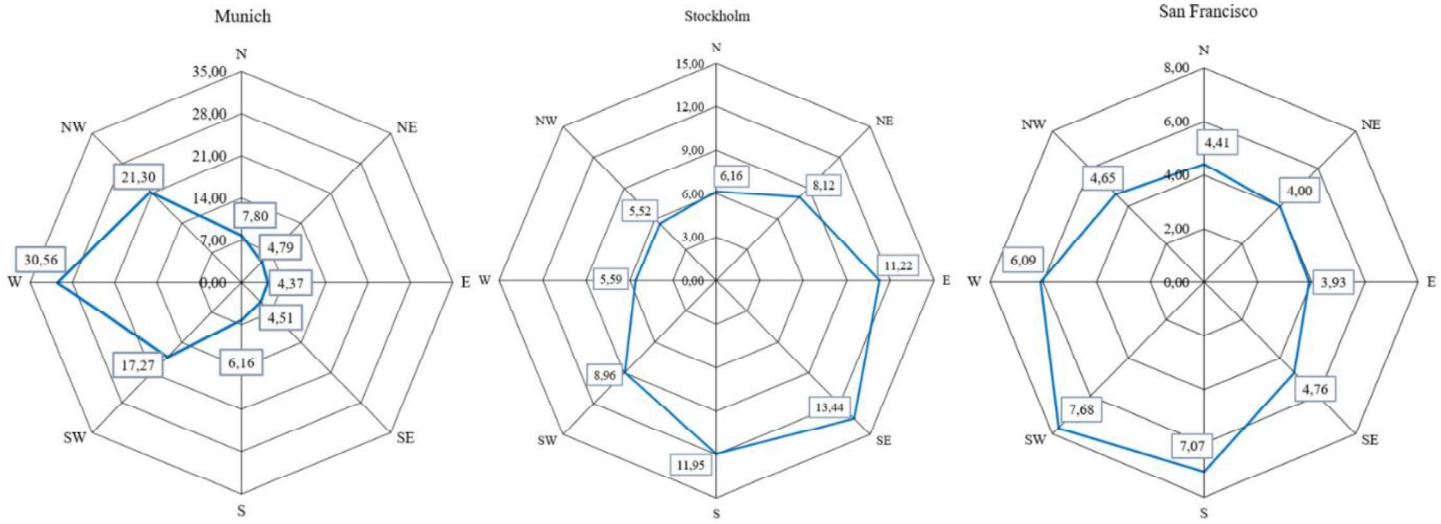

Figure 4. Annual average water content (kg/m^3) as a function of wall orientation.

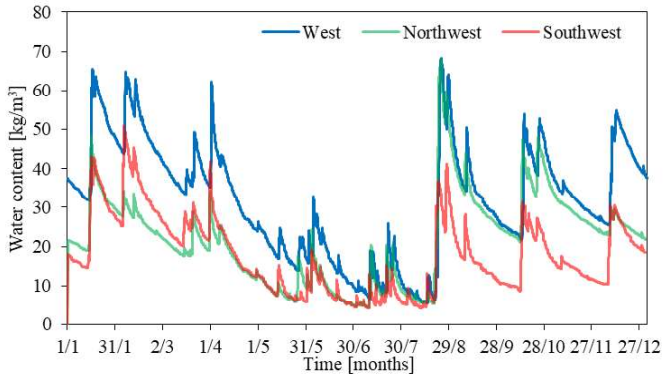

Figure 5. Variation of water content for the western (blue), northwestern (green), and southwestern (red) facades in Munich.

3.1.2 Comparison between the three climates

Exterior masonry walls are subjected to cycles with a wetting phase (increase of water content) and drying phase (decrease of water content). The duration of these cycles depends, not only on the wall assembly, but also the boundary conditions [12]. Figure 6a, b, and c display the variation of water content as a function of wall thickness in each of the three studied climates. In Munich, the wetting phase occurs from the middle of August to the middle of January. In Stockholm, the wetting phase occurs from middle of September to the beginning of January. In San Francisco, the wetting phase occurs from the beginning of November to the end of March.

The results show that an increase in wall thickness leads to higher water content values, as well as a generally slower drying processes, due to the increased *water vapor diffusion equivalent air layer thickness* (S_d-value). As expected, in Munich,

wall thickness has a more significant effect on the water content values attained, due to the higher wind-driven rain loads.

Conversely, the values attained in Stockholm are generally higher than San Francisco (see Figure 6d), even though both climates have similar wind-driven rain loads. This behavior is due to two main factors: firstly, the higher amount of solar radiation in San Francisco, as well as the exterior air temperature, which results in an enhanced drying potential; secondly, in San Francisco, the exterior air temperature never drops below the freezing point, unlike Stockholm (see Table 2). Under these conditions, wind-driven rain is no longer responsible for an increase of water content, since there is no capillary suction below 0 ºC [15].

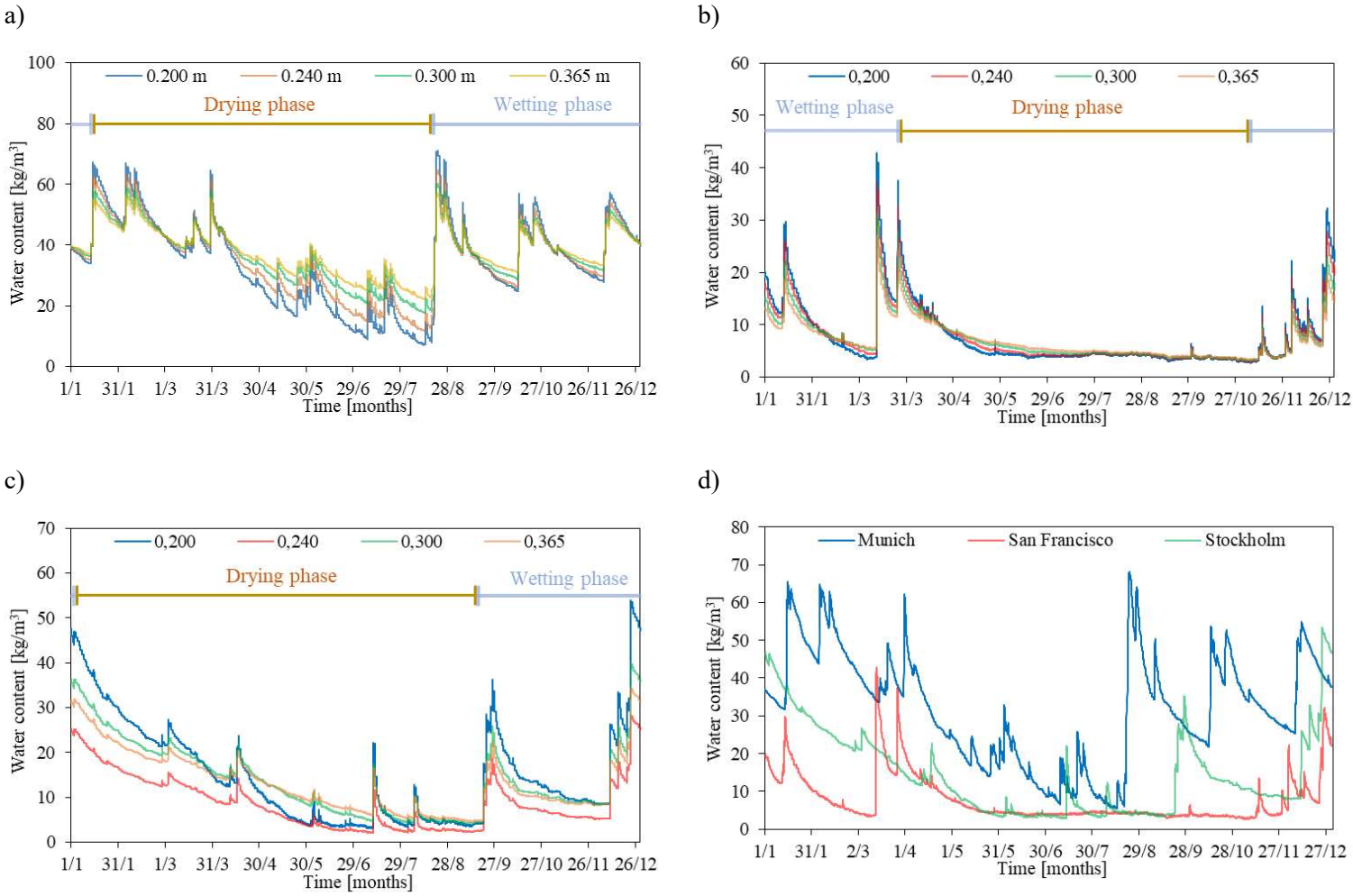

Figure 6. Variation of water content as a function of wall thickness in Munich (a), San Francisco (b), and Stockholm (c) and variation of water content for the standard case (0.2 m block) in the three studied climates (d).

Table 3 shows the thermal transmittance variance between the steady-state and transient state models for the standard case (i.e. 200 mm). The results indicate that calculating the thermal transmittance in steady-state conditions can lead to gross underestimations of the transient value. The difference in thermal transmittance is highest in Munich during the wetting phase (31.6 %) and lowest in San Francisco during the drying phase (4.6 %). This difference is lower if you consider the thermal resistance (23.9 % in Munich and 4.4 % in San Francisco). This behavior is understandable if equation (1) is taken

into account, due to the water content values achieved in these climates. These results further support the notion that the thermal conductivity of AAC is highly moisture dependent.

Table 3. Thermal transmittance variance for the standard case (i.e. 200 mm) in Munich, Stockholm, and San Francisco.

Case	U_{WUFI}	Annual		Wetting Phase		Drying Phase	
	[W/m^2 K]	U_A [W/m^2 K]	Relationship	U_W [W/m^2 K]	Relationship	U_D [W/m^2 K]	Relationship
Munich	0.458	0.586	27.9%	0.602	31.4%	0.574	25.3%
Stockholm		0.514	12.2%	0.550	20.1%	0.492	7.4%
San Francisco		0.487	6.3%	0.499	9.0%	0.479	4.6%

3.1.3 Frost damage potential on the AAC layer

In San Francisco, the exterior air temperature does not drop below the freezing point, and thus, no ice formation occurs in the AAC layer. Figure 7 displays the total and critical number of freeze-thaw cycles as a function of orientation in Munich and Stockholm. The results show that orientation has a significant influence on the critical number of freeze-thaw cycles, given that the façade with the highest wind-driven rain load also reaches the highest number of critical cycles (i.e. western façade in Munich and southeastern façade in Stockholm).

Furthermore, according to the frost indexes (Time-of-Frost and Amount-of-Frozen-Water), these cases are also the most susceptible to frost damage (Table 4), which is indicative of the influence wind-driven rain has on potential frost damage. However, solar radiation also plays a significant role. When analyzing the total number of freeze-thaw cycles that occur, the southern facades show a higher number of cycles relative to the northern facades. This behavior is due to the higher amount of solar radiation on the southern facades (see Figure 3), leading to a more pronounced variation of the exterior surface temperature and, thus, the number of zero crossings on the Celsius scale (Figure 8).

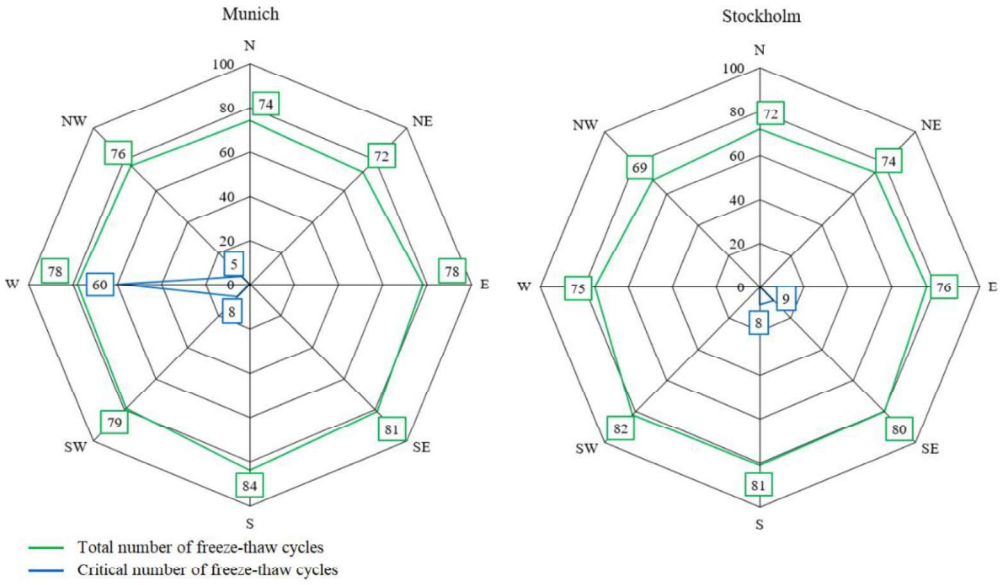

Figure 7. Total (green) and critical number (blue) of freeze-thaw cycles as a function of wall orientation.

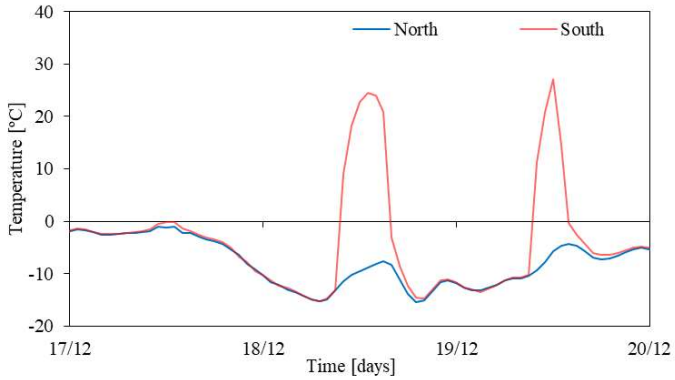

Figure 8. Variation of exterior surface temperature for the north- (blue) and south- (red) oriented facades in Munich from the 17th to the 20th of December.

Table 4. Frost damage analysis in Munich and Stockholm.

Climate	Orientation	Freeze-thaw cycles [-]	Time of Frost [h]	Amount of Frozen Water [kg/m^3]	Wind-driven rain [l/m^2.a]
Munich	West	60	841	40 738	232.8
	Southwest	8	80	3 136	180.4
	Northwest	5	76	3 134	180.2
Stockholm	Southwest	9	297	13 447	72.9
	South	8	283	12 157	68.1

3.2 Changes imposed by the application of the render and plaster layer

3.2.1 Render material

Figure 9a, b, and c show the water content variation for an AAC wall with interior gypsum plaster and three different exterior renders: lime, lime-cement, and cement renders. In order to identify the changes imposed by the application of the aforementioned layers, an unrendered AAC wall is also represented, i.e. the standard case. The average annual water content for each study case can be seen in Table 5.

In Munich, the results show that the lime and lime-cement rendered walls exhibit higher water contents relative to the standard case. In Stockholm and San Francisco, the application of a lime render causes a slight increase in water content, whereas the lime-cement render causes a slight decrease. The cement rendered walls show a significant decrease in water content in all studied climates.

Table 5. The AAC layer's average annual water content for the three selected climates.

Render material	Munich		San Francisco		Stockholm	
	Water content [kg/m^3]	Relationship	Water content [kg/m^3]	Relationship	Water content [kg/m^3]	Relationship
Standard case	31.9	–	7.7	–	13.4	–
Lime	39.8	24.8%	8.8	14.9%	14.7	9.5%
Lime-cement	44.9	40.9%	7.0	-8.9%	12.0	-10.7%
Cement	5.0	-84.2%	4.1	-47.2%	5.2	-61.6%

In order to understand the increase in water content for the lime and lime-cement rendered walls in Munich, these cases were further analyzed during the first two years of the simulation period (Figure 9d). According to the results, these renders seem to perform adequately during the first couple of months of the simulation period, given that there is a general decrease in water content. This is due to the lower water absorption coefficient of these renders relative to the AAC block (see Table 1), resulting in a lower liquid flux towards the interior of the wall.

However, there is also an accumulation of moisture as the simulation period occurs, eventually surpassing the water content values attained in the standard case. This behavior can be attributed to two main factors. Firstly, application of the render and plaster layers leads to an increase of the water vapor diffusion equivalent air layer thickness (S_d-value), and as a result, the moisture inside the building material has greater difficulty evaporating through both faces of the constructive element. Secondly, the liquid transport coefficient is highly influenced by the amount of moisture inside the building components [15].Therefore, higher water content values lead to a greater liquid flux density towards the constructive elements. On the other hand, the cement render causes such a significant reduction of the liquid transport coefficient of the exterior surface that the increase of the vapor diffusion resistance has hardly any influence on the drying potential of the wall (Figure 9a, b, and c).

a)

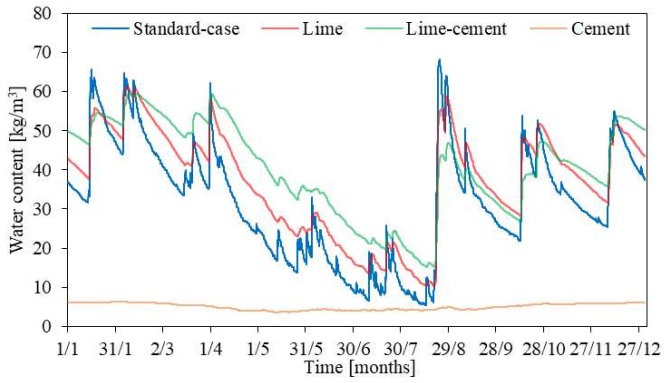

b)

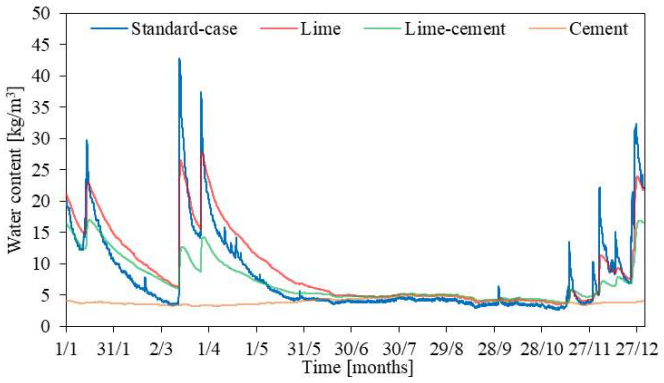

c)

d)

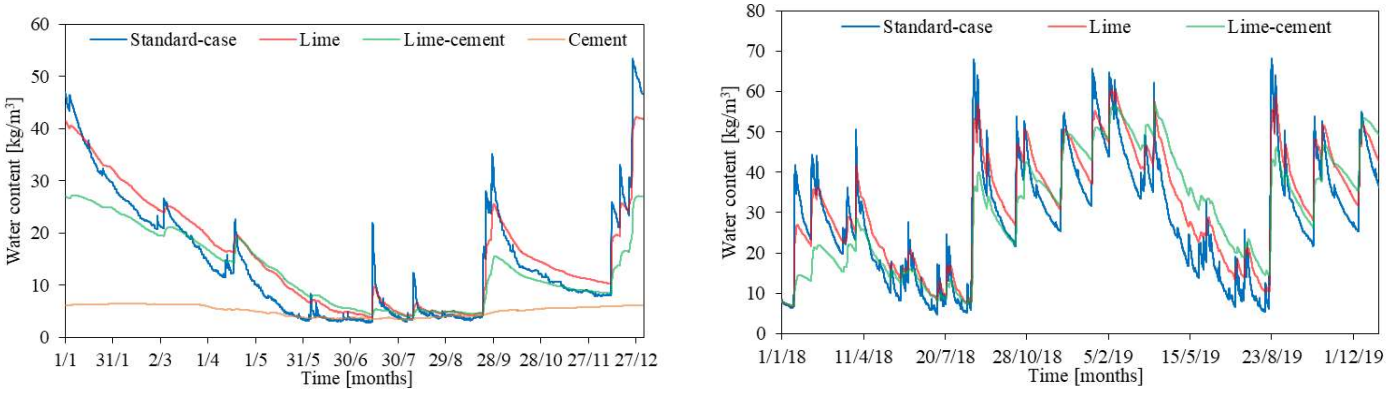

Figure 9. Variation of water content for each study case in Munich (a), San Francisco (b), Stockholm (c) for the standard case (blue), lime (red), lime-cement (green), and cement (yellow) rendered walls during the reference year and the variation of water content for the lime and lime-cement rendered walls in Munich during the first two years of simulation (d).

The influence of render thickness on water content was also analyzed. The results showed that an increase in render thickness leads to a lower variation of water content, due to the increased vapor diffusion resistance and reduced drying potential of the masonry wall. However, the difference in water content for the lime rendered and cement rendered walls was negligible, unlike the lime-cement rendered wall (see Figure 10).

The lime render has a relatively low water vapor diffusion resistance factor (i.e. 7), so the drying potential of the wall was not significantly affected by the thickness of the exterior render. The cement render has the highest water vapor diffusion resistance factor (i.e. 25); however, it also has the lowest liquid transport coefficient (see Table 1). As a result, the exterior liquid flux is greatly reduced, and the water content values achieved are minimal. Conversely, the thickness of the lime-cement render was shown to have a significant influence on water content, due to its relatively high water vapor diffusion resistance factor (i.e. 19), which coupled with the high water content values achieved, greatly affecting the drying potential of the masonry wall.

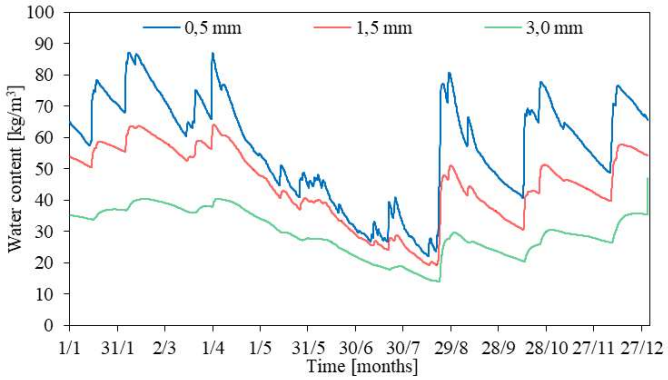

Figure 10. Variation of water content as a function of render thickness in Munich for the lime-cement rendered wall.

Figure 11 shows the annual variation of thermal transmittance for each study case in Munich. The cement render leads to a significant reduction of thermal transmittance, whereas the lime and lime-cement renders cause a slight increase. As shown, the application of these renders causes an increase in water content due to the reduced drying potential of the wall. If the

AAC layer reaches high water content values, due to inadequate performance of the exterior render, then, the thermal transmittance of the wall assembly can be significantly impaired. In this context, the properties of the exterior render greatly influence the thermal transmittance of the AAC masonry wall, namely the liquid transport coefficient and water vapor diffusion resistance factor.

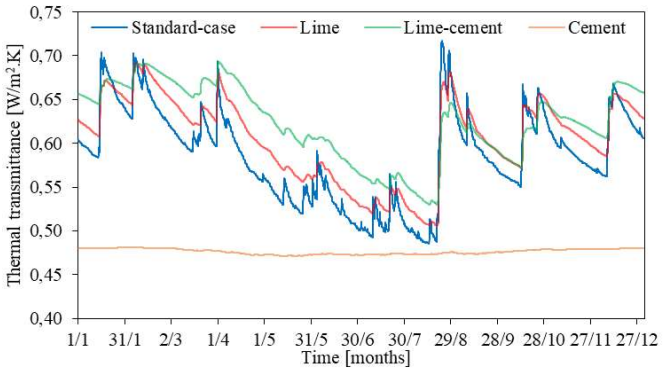

Figure 11. Variation of thermal transmittance for each study case in Munich.

3.2.2 Frost damage potential on the rendered AAC layer

Table 6 shows the results for potential frost damage on the AAC layer after the application of plaster and render in Munich. The results show that the cement render completely eliminates the occurrence of critical freeze-thaw cycles in the AAC layer, due to the low water content values achieved, which consistently stay below the capillary region. As a result, ice formation no longer causes damage to the pore structure of the AAC.

On the other hand, the lime and the lime-cement renders only cause a slight reduction of two critical freeze-thaw cycles, down to a total of 58 cycles per year. Although this behavior may seem satisfactory at first, the TOF and AFW damage functions show that the occurrence of these cycles are more damaging to the AAC layer, due the higher water content values achieved, which may lead to faster degradation of the material.

As shown before, the lime and lime-cement renders are responsible for an increase of water content in the AAC layer due to their inability to adequately protect the masonry against moisture entry, unlike the cement render (Figure 9). As a result, ice formation occurs in the AAC layer when its pores are closer to saturation, leading to a greater frost damage potential. In Stockholm, the application of a plaster and render layer eliminated the occurrence of critical freeze-thaw cycles.

Table 6. Frost damage analysis for a rendered AAC wall in Munich.

Study case	Critical freeze-thaw cycles	Time of Frost	Amount of Frozen Water
	[-]	[h]	[kg/m^3]
Standard case	60	841	40 738
Lime	58	1 026	49 616
Lime-cement	58	984	50 817

Cement	0	0	0

3.3 Changes imposed by the application of an ETICS system

3.3.1 Rainwater leakage

Moisture control in building components has always been a priority due to the numerous anomalies that can arise from rainwater leakage. The recent evolution in numerical simulation software to model the hygrothermal behavior of constructive solutions has sparked a renewed interest in the water tightness of masonry walls. Unfortunately, most hygrothermal models assume a perfectly assembled wall system, without any cracks or gaps that would allow for unforeseen moisture entry [23].

In order to identify the changes in water content resulting from rainwater leakage in AAC masonry walls, a comparison between three ETICS systems was carried out (i.e. MW, EPS, and XPS). Different rainwater leakage values were analyzed: 0% of wind-driven rain, assuming a perfectly watertight system without any cracks or gaps; 1 %, the default value according to ANSI/ASHRAE Standard 160; 3 %; and 5 %, assuming a worst-case scenario [25].

Figure 12 shows the variation of water content for each study case (MW, EPS, and XPS) as a function of rainwater leakage in Munich. The results show rainwater leakage has minimal influence on the water content of the MW insulated wall, contrary to the EPS and XPS systems. This behavior is due to the lower water vapor diffusion resistance factor of MW, resulting in a higher vapor transport towards the exterior. For this reason, the MW insulated wall dries significantly faster than the EPS and XPS insulated walls. The same results were attained in Stockholm and San Francisco, differing only in magnitude, due to the lower wind-driven rain loads.

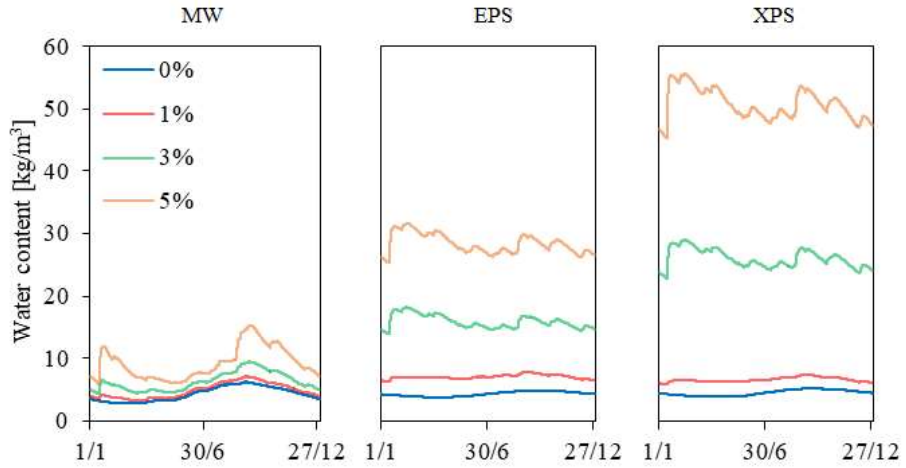

Figure 12. Variation of water content as a function of rainwater leakage for the MW, EPS, and XPS insulated walls in Munich.

3.3.2 Insulation material

Figure 13a, b, and c display the variation of water content as a function of insulation material in Munich, San Francisco, and Stockholm. According to the results, the insulation material has minimal influence on water content. However, the MW insulated wall reaches the lowest values, overall, followed by the EPS and XPS systems. This behavior is due to the lower

water vapor diffusion resistance factor of the MW insulation, resulting in a higher vapor diffusion flux towards the exterior and, thus, an enhanced drying potential.

It is also possible to conclude that the application of an ETICS system causes a gap between the previous drying and wetting phases, since water content is no longer influenced by periods of precipitation but by the interior relative humidity, instead. The reason for this behavior can be attributed to two main factors. Firstly, the insulation materials simulated are non-hygroscopic materials, and thus, they form a natural barrier to moisture entry [15]. Secondly, the reduced liquid transport coefficient of the exterior resin finish, coupled with its high water vapor diffusion resistance factor (see Table 1), substantially reduces moisture flux towards the interior of the constructive element. The combination of these factors significantly reduces the amount of moisture that results from wind-driven rain, even when considering rainwater leakage through the ETICS system. Under these circumstances, the water content of the AAC layer is now primarily influenced by the interior relative humidity.

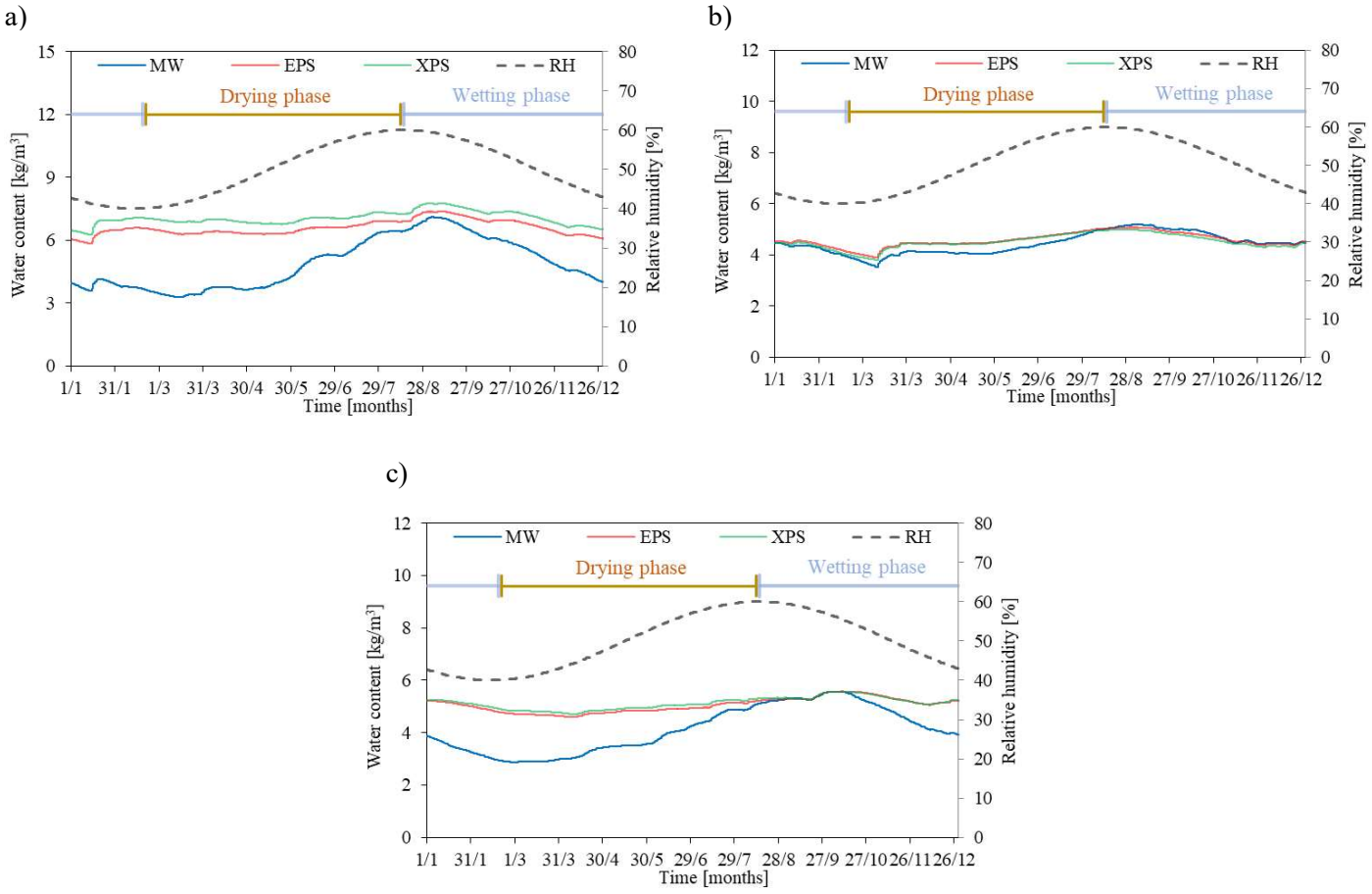

Figure 13. Variation of water content in the AAC layer for the MW (blue), EPS (red), and XPS (green) ETICS in Munich (a), San Francisco (b), and Stockholm (c).

4. Conclusions

The work presented herein aimed at identifying the influence of climatic conditions on the hygrothermal performance of AAC wall systems. This was achieved by simulating several constructive solutions on different climatic settings, from

which the main conclusions are summarized, as follows:

- The hygric properties of the exterior render significantly influence the overall hygrothermal performance of AAC masonry walls. However, the importance of these properties varies according to climatic conditions. In Munich, the application of a lime-cement render led to a significant increase in water content (41 %), whereas in Stockholm and San Francisco, it led to a slight decrease (11 % and 9 %, respectively).
- The results showed that calculating the thermal transmittance of AAC masonry walls in steady-state conditions can lead to gross underestimations compared to transient models. Moreover, thermal transmittance of the masonry was found to be greatly influenced by the hygrothermal properties of the exterior render, namely the water absorption coefficient and water vapor diffusion resistance.
- When analyzing the AAC masonry from the point-of-view of possible frost damage, wind-driven rain assumes a critical role. Additionally, the severity of frost damage on the AAC block was found to be significantly dependent on the orientation of the facade. The number of critical freeze-thaw cycles was also shown to be influenced by solar radiation, given that there was typically a higher number of cycles for the south-oriented facades.

Acknowledgments

The authors acknowledge the support of *Fraunhofer Institute for Building Physics* by providing a student license for the simulation tool *WUFI® Pro*. The authors acknowledge the FCT – Fundação para Ciência e a Tecnologia – for the financial support through the PhD scholarships PD/BD/127844/2016.

References

[1] N. Narayanan, K. Ramamurthy, Structure and properties of aerated concrete: a review, Cement and Concrete Composites. 22 (2000) 321–329. doi:10.1016/S0958-9465(00)00016-0.

[2] H. Kus, P. Norberg, Evaluation of the long-term performance of water repellants on rendered autoclaved aerated concrete, (1999) 1031. doi:10.1007/978-3-642-37475-3.

[3] M. Jerman, M. Keppert, J. Výborný, R. Černý, Hygric, thermal and durability properties of autoclaved aerated concrete, Construction and Building Materials. 41 (2013) 352–359. doi:10.1016/j.conbuildmat.2012.12.036.

[4] V. Kočí, J. Maděra, R. Černý, Exterior thermal insulation systems for AAC building envelopes: Computational analysis aimed at increasing service life, Energy and Buildings. 47 (2012) 84–90. doi:10.1016/j.enbuild.2011.11.030.

[5] R. Drochytka, J. Zach, A. Korjenic, J. Hroudová, Improving the energy efficiency in buildings while reducing the waste using autoclaved aerated concrete made from power industry waste, Energy and Buildings. 58 (2013) 319–323. doi:10.1016/j.enbuild.2012.10.029.

[6] X. Qiu, F. Haghighat, M.K. Kumaran, Moisture Transport Across Interfaces Between Autoclaved Aerated Concrete and Mortar, Journal of Thermal Envelope and Building Science. 26 (2003) 213–236. doi:10.1177/109719603032804.

[7] H. Künzel, Criteria Defining Rain Protecting External Rendering Systems, Energy Procedia. 78 (2015) 2524–2529. doi:10.1016/J.EGYPRO.2015.11.260.

[8] Fraunhofer-IBP, WUFI 6.1-PRO, (2017).

[9] B. Villmann, V. Slowik, F.H. Wittmann, P. Vontobel, J. Hovind, Time-dependent Moisture Distribution in Drying Cement Mortars – Results of Neutron Radiography and Inverse Analysis of Drying Tests, Restoration of Buildings and Monuments. 20 (2014) 49–62. doi:10.12900/rbm14.20.1-0004.

[10] Ü. Alev, T. Kalamees, M. Teder, M.-J. Miljan, Air leakage and hygrothermal performance of an internally insulated log house, in: NSB 2014 10th Nordic Symposium on Building Physics, 2014: pp. 55–62.

[11] M.L.M. Nascimento, E. Bauer, J.S. de Souza, V.A.G. Zanoni, Wind-driven rain incidence parameters obtained by hygrothermal simulation, Journal of Building Pathology and Rehabilitation. 1 (2016) 1–7. doi:10.1007/s41024-016-0006-5.

[12] G.B.A. Coelho, F.M.A. Henriques, Influence of driving rain on the hygrothermal behavior of solid brick walls, Journal of Building Engineering. 7 (2016) 121–132. doi:10.1016/j.jobe.2016.06.002.

[13] N.M. Ramos, J.Q. Delgado, E. Barreira, V.P. de Freitas, Hygrothermal properties applied in numerical simulation: Interstitial condensation analysis, Journal of Building Appraisal. 5 (2009) 161–170. doi:10.1057/jba.2009.27.

[14] Cen, EN 15026, Hygrothermal performance of building components and building elements - Assessment of moisture transfer by numerical simulation, 2007.

[15] H. Künzel, Simultaneous Heat and Moisture Transport in Building Components One-and two-dimensional calculation using simple parameters, Fraunhofer IRB Verlag Suttgart. (1995).

[16] K. Calle, N. Van Den Bossche, Analysis of different frost indexes and their potential to assess frost based on HAM simulations, in: ProXIV DBMC 14th INternational Confernce On Durability of Buildings Materials and Components, RILEM Publications S.A.R.L., 2017: pp. 61–62.

[17] J. Kočí, J. Maděra, M. Keppert, R. Černý, Damage functions for the cold regions and their applications in hygrothermal simulations of different types of building structures, Cold Regions Science and Technology. 135 (2017) 1–7. doi:10.1016/j.coldregions.2016.12.004.

[18] V. Kočí, J. Výborný, R. Černý, Computational and experimental characterization of building envelopes based on autoclaved aerated concrete, in: WIT Transactions on Engineering Sciences, WIT Press, 2011: pp. 363–373. doi:10.2495/MC110321.

[19] V. Kočí, J. Maděra, R. Černý, Computer aided design of interior thermal insulation system suitable for autoclaved aerated concrete structures, Applied Thermal Engineering. 58 (2013) 165–172. doi:10.1016/j.applthermaleng.2013.04.023.

[20] J. Straube, C. Schumacher, Assessing the durability impacts of energy efficient enclosure upgrades using hygrothermal modeling, Journal of the International Association for Science and Technology of Building Maintenance and Monuments Preservation. 2 (2006) 197–222.

[21] H. Künzel, H.M. Künzel, K. Sedlbauer, Long-term performance of external thermal insulation systems (ETICS), ACTA Architectura. 5 (2006) 11–24.

[22] H. Bagheri, B.G. Hellers, Prestressed AAC masonry in prefabrication of a new building, in: 14th International Brick and Block Masonry Conference, Sidney, 2008.

[23] H.M. Künzel, D. Zirkelbach, Advances in hygrothermal building component simulation: Modelling moisture sources likely to occur due to rainwater leakage, Journal of Building Performance Simulation. 6 (2013) 346–353. doi:10.1080/19401493.2012.694911.

[24] ASHRAE, ASHRAE standard 160P - Criteria for moisture control design analysis in buildings, 2008. http://sspc160.ashraepcs.org/ (accessed June 28, 2017).

[25] N. Van Den Bossche, M. Lacasse, A. Janssens, Watertightness of Masonry Walls : An Overview Introduction Brick cavity walls, 12th International Conference on Durability of Building Materials and Components, Proceedings. (2011) 1–8.

[26] Institut Für Bauklimatik-Dresden, Delphin - version 6.0.20, (n.d.).

[27] V.P. De Freitas, V. Abrantes, P. Crausse, Moisture migration in building walls—Analysis of the interface

phenomena, Building and Environment. 31 (1996) 99–108. doi:10.1016/0360-1323(95)00027-5.

[28] M. Kottek, J. Grieser, C. Beck, B. Rudolf, F. Rubel, World Map of the Köppen-Geiger climate classification updated, Meteorologische Zeitschrift. 15 (2006) 259–263. doi:10.1127/0941-2948/2006/0130.

[29] H.M. Künzel, Effect of Interior and Exterior Insulation on the hygrothermal behaviour of exposed walls, Materials and Structures. 31 (1988) 99–103.